

Article

Optical Lines in Europium and Terbium-Activated Yttrium Tantalate Phosphor: Combined Experimental and Group-Theoretical Analysis

Michael Nazarov ¹ and Boris Tsukerblat ^{2,*} 

¹ Institute of Applied Physics, Moldova State University, Academy Street 5, MD-2028 Chisinau, Moldova; mvnazarov@mail.ru

² Department of Chemistry, Ben-Gurion University of the Negev, Beer-Sheva 84105, Israel

* Correspondence: tsuker@bgu.ac.il

Abstract: The rare-earth ions in crystals such as terbium (YTaO₄:Tb³⁺) and europium (YTaO₄:Eu³⁺)-activated yttrium tantalate phosphors have a number of attractive features that predetermine their crucial role in practical application in contemporary optoelectronic devices. In this article, we employ the group-theoretical arguments aimed to reveal the group-theoretical classification of the crystal field levels and selection rules for the allowed optical transition between the crystal field components of Tb³⁺ and Eu³⁺ of the low symmetry crystal field in the activated yttrium tantalate phosphors. We also establish possible polarization rules for the lines corresponding to the allowed transitions. We deduce the symmetry-assisted results for the selection rules in the optical transitions accompanied by the absorption/emission of the vibrational quanta. The selection rules for the vibronic satellites of the zero-phonon lines are expected to be useful for the identification of the lines in the spectra of rare-earth ions with a weak vibronic coupling. The results of the low-temperature measurements of photoluminescence under the 325 nm excitation are in compliance with the group-theoretical analysis. The aim of the paper is to establish symmetry-assisted results that are the background of the quantitative crystal field theory based on the quantum-mechanical consideration.

Keywords: symmetry; crystals YTaO₄:Eu³⁺, Tb³⁺; photoluminescence; Stark levels; polarization rules; vibronic satellites



Citation: Nazarov, M.; Tsukerblat, B. Optical Lines in Europium and Terbium-Activated Yttrium Tantalate Phosphor: Combined Experimental and Group-Theoretical Analysis.

Optics **2023**, *4*, 510–524. <https://doi.org/10.3390/opt4030037>

Academic Editor: Young-Ki Kim

Received: 7 August 2023

Revised: 26 August 2023

Accepted: 31 August 2023

Published: 7 September 2023



Copyright: © 2023 by the authors. Licensee MDPI, Basel, Switzerland. This article is an open access article distributed under the terms and conditions of the Creative Commons Attribution (CC BY) license (<https://creativecommons.org/licenses/by/4.0/>).

1. Introduction

Among highly efficient luminescent materials, the yttrium tantalate the crystals (YTaO₄) should be specially mentioned. It is well known that non-activated YTaO₄ is an efficient X-ray phosphor. The role of these phosphors is to reduce the exposure of the patient to X-rays while preserving the structural features of the X-ray image. The pronounced luminescence can be initiated through various kinds of excitation such as UV light cathode radiation or X-ray. Although the structure of YTaO₄ was studied by Walten [1] and Brixner and Chen [2] half a century ago, these crystals still attract the attention of researchers due to their role in different practical applications, for example, in contemporary optoelectronic devices. Studies continued on both undoped YTaO₄ [3] and activated YTaO₄ with various rare-earth elements [4–7], including those with double activation [7–9].

The first reason for continuing investigation of these phosphors is to study the mechanism of Eu³⁺ and Tb³⁺ luminescence in the tantalite matrix lattice. The study of the rare-earth ions in crystals such as terbium and europium-activated yttrium tantalate phosphors (YTaO₄:Tb³⁺, YTaO₄:Eu³⁺) has been the subject of a large number of both experimental and theoretical works reflected in numerous publications [7–12]. The number of publications increases every year, as many observed phenomena have not found their explanation. Yttrium tantalates play a role of self-activated crystals because they can be used as a host that adopts the rare-earth ions that have interesting and practically useful properties. One

must specially emphasize a possibility of efficient transfer of the excitation energy between impurity ions of different natures in these crystals. The charge transfer leading to luminescence of YTaO_4 -doped either with Tb^{3+} or with Eu^{3+} ions was first demonstrated by Blasse and co-workers [13–15]. They showed that charge transfer results in a strong luminescence band in green area of $\text{YTaO}_4:\text{Tb}^{3+}$ crystals under UV, VUV, CL, and X-ray excitation. Under the same types of excitation, the Eu^{3+} -doped YTaO_4 crystals exhibit a red emission band. It is to be noted that both phosphors are efficient materials in different applications [16], such as optoelectronic devices. The growing interest towards luminescence properties in a wide spectral range is closely interrelated with prospects for the new promising applications that stimulated the development of this area. Despite the fact that YTaO_4 itself is a well-known self-activating phosphor, europium and terbium-activated yttrium tantalates and their electronic structure, the mechanism of optical absorption, and optical transitions are not fully understood. The main stimulus for the study of this phosphor is an attempt to achieve a better understanding of the mechanism of luminescence and optical transitions, taking into account the splitting of ion levels caused by the crystal field. Due to complicated structure of the sites occupied by the impurity ions found in the quantum-chemical studies of these systems, the number of the crystal field parameters is rather large. Under this condition, the use of the symmetry properties of the system can bring important information that can be supported by ab initio calculations of the crystal field parameters. In this view, the polarization selection rules in the optical transitions in doped phosphors so far mentioned can be useful.

The study of the optical spectra of impurity ions is usually reduced to two stages. The first one is the group-theoretical study of possible energy levels of an ion in the crystal field that includes derivation of the irreducible representations (irreps) to which the levels belong to as well as the selection rules predetermining number and intensities of the crystal field optical pattern. These data, based exclusively on the symmetry of the site and wave function of the impurity ion, are to be used at the second step of the study that includes quantum-mechanical evaluation of the crystal field parameters and consequently crystal field levels. For example, the number of states with the repeated irreducible representations determines the size of the energy matrices to be diagonalized. In this article, we solve the first problem focused on the symmetry properties.

This paper is devoted to the study of the selection rules in YTaO_4 -doped by Tb^{3+} and Eu^{3+} for the optical transitions in different polarizations because polarization selection rules and optical transitions in this type of materials have not been studied yet in detail. We also discuss the interpretation of their photoluminescence (PL) spectra under 325 nm excitation at 10 K. The theoretical symmetry-based calculations allow us to better understand the fine structure of emission transitions at low temperatures. Finally, we discuss further perspectives for the applications of symmetry-assisted theoretical approaches to the analysis of the terbium and europium-activated yttrium tantalate phosphors $\text{YTaO}_4:\text{Tb}^{3+}$, $\text{YTaO}_4:\text{Eu}^{3+}$.

2. Materials and Methods

2.1. Preparation of Samples

Terbium-activated yttrium tantalate $\text{Y}_{0.95}\text{Tb}_{0.05}\text{TaO}_4$ and europium-activated $\text{Y}_{0.95}\text{Eu}_{0.05}\text{TaO}_4$ samples were prepared by solid state reaction. The incorporation of Tb^{3+} and Eu^{3+} into the monoclinic crystal lattice of YTaO_4 proves to be possible due to the proximity of the ionic radii of the activators and Y^{3+} in the host lattice in six-fold coordination [17,18]. A wide set of experimental data on the crystals having this structure are described in detail in the book [19]. Therefore, we will not give more details here. The influence of the flux nature and photoluminescent properties was investigated and Na_2SO_4 (99%) as flux was chosen as the best. The activator concentrations used and the main synthesis parameters are based on our previous works [6,19].

The reaction uses homogeneous mixtures of Y_2O_3 (99.9%) and Ta_2O_5 (Optipur) as oxide precursors for the host lattice, and Eu_2O_3 and/or Tb_4O_7 as activator system. The

stoichiometric amounts of Y_2O_3 , Ta_2O_5 , and/or Eu_2O_3 and/or Tb_4O_7 together with 30 wt.% alkaline sulphates were ball-milled with acetone and dried at 70 °C. The planetary-mill of pulverisette type using agate balls and mill-beaker set was used to prepare the reactive oxide–flux mixture. The 5 mol% activator concentration was optimal. The powder mixture was baked in air at 1200 °C for 4 h and then cooled down to room temperature. At the final stage, the samples of the phosphor were water washed, dried, and sieved. The photoluminescence initiated by He–Cd laser at 325 nm was employed for the sample characterization. The measurements of the optical spectra were performed at low temperature (10 K) and then compared with room temperature data.

2.2. Crystal Structure of Yttrium Tantalate-Activated by Terbium ($YTaO_4:Tb^{3+}$) and Europium ($YTaO_4:Eu^{3+}$)

The $YTaO_4$ crystalline matrix has long been known as a self-activating phosphor. Performances of these phosphors are related to composition, crystalline structure, particle dimensions, and luminescence properties of powders. Both natural fergusonite (yttrium-niobium tantalate) and synthetic $YTaO_4$ crystallize in monoclinic symmetry and have space group $I2/a$, with yttrium tantalate $YTaO_4$ having three types of crystal structure. The high-temperature tetragonal form (T) with a scheelite structure is distorted by a second-order phase transition at a temperature of about 1450 °C, into a monoclinic (M) structure having a fergusonite structure. We have discussed in detail the structure of M' - $YTaO_4$ that gives rise to the most intensive light emission. Due to the second-order phase transition, the scheelite structure is distorted into a high-temperature tetragonal form (T). At temperatures below 1400 °C another monoclinic structure, called M' , can be directly synthesized. We consider in this work just this modification M' because it is much brighter in comparison M and T structure, and shown in Figure 1. As a new structure type, M' $YTaO_4$ was first described by Wolten [1] and then improved by Brixner and Chen [2]. The average Y–O distance in $YTaO_4$ is 2.355 Å. The tantalum atoms are in a distorted octahedral coordination with four shorter Ta–O bonds at 1.86 and 1.95 Å, and two longer ones at 2.23 Å. The unit cell parameters are $a = 5.30$, $b = 5.45$, $c = 5.11$ Å, and $\beta = 96.5^\circ$. These distorted TaO_6 units share edges to form strings. Yttrium, in eight-fold coordination with oxygen, interconnects the Ta–O strings.

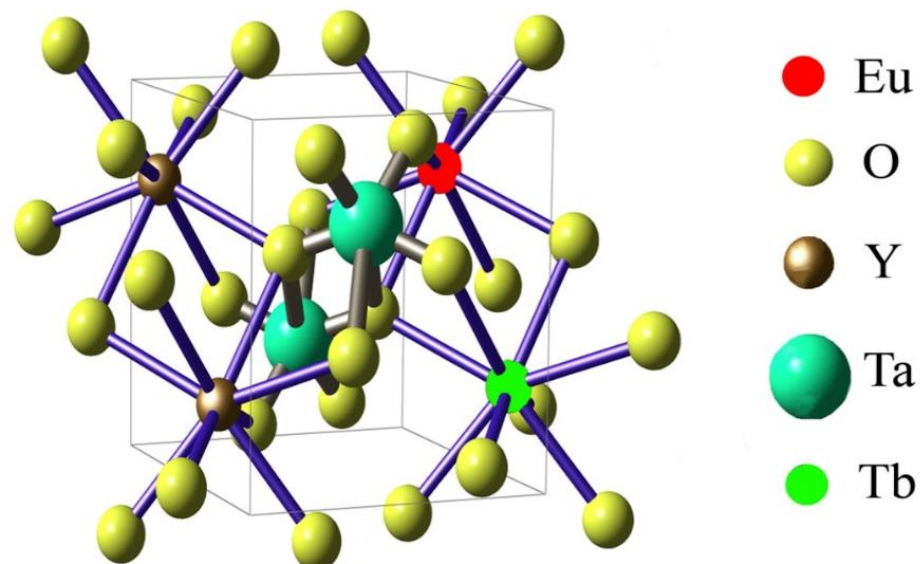


Figure 1. Crystal structure of M' - $YTao_4$ doped with Eu^{3+} activation (red), or Tb^{3+} activation (green), or double activation by Eu^{3+} and Tb^{3+} [19]. (Reprinted with permission from [20]. Copyright 1995: Elsevier).

In M' - $YTao_4$ -doped by Eu^{3+} or Tb^{3+} , the Y atoms are substituted by Eu^{3+} or Tb^{3+} and they are surrounded by eight-coordinated oxygen atoms, forming a distorted cube with

averaged Y-O distance 2.37 Å. The Ta atoms have distorted octahedral coordination with four shorter Ta-O bonds (1.96 Å and 1.87 Å) and two longer ones (2.23 Å). The M' - $YTaO_4$ structure contains two yttrium atoms, two tantalum atoms, and eight oxygen atoms.

2.3. Low-Temperature Photoluminescence Measurements

The scheme of the experimental setup used in the low-temperature measurements of photoluminescence (PL) is shown in Figure 2.

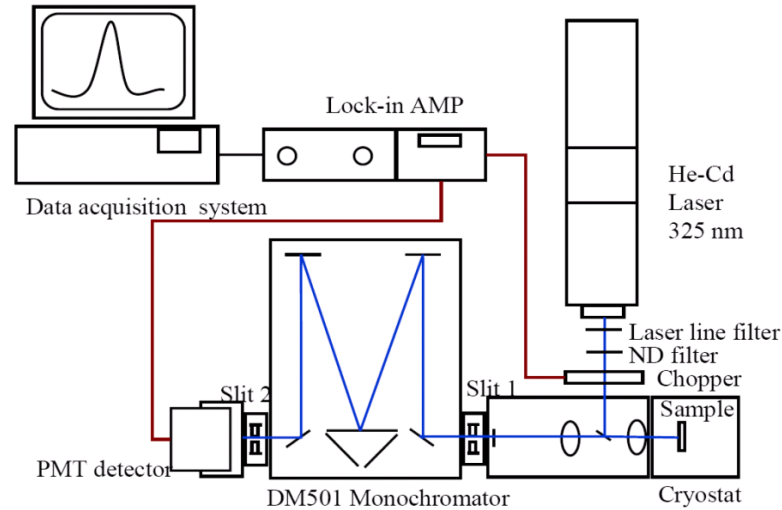


Figure 2. Scheme of the experimental setup for the PL measurement.

In the low-temperature experiments, we used the following measurement conditions: Source-325 nm He-Cd laser, Detector-PMT, Grating-1200 gr/mm, Scan Range: 450–720 nm, Slit size: 0.03 mm, Step: 0.05 nm, Temperature-10 K.

3. Results

3.1. Experimental Results for $YTaO_4:Tb^{3+}$

All experiments were performed at low temperature 10 K, because at room temperature, the spectra are poorly resolved and the fine structure is not visible. We made such measurements at room temperature in our previous works [6,19]. The general pattern of the emission spectrum of $YTaO_4:Tb^{3+}$ initiated by 325 nm He-Cd laser excitation at 10 K is presented in Figure 3.

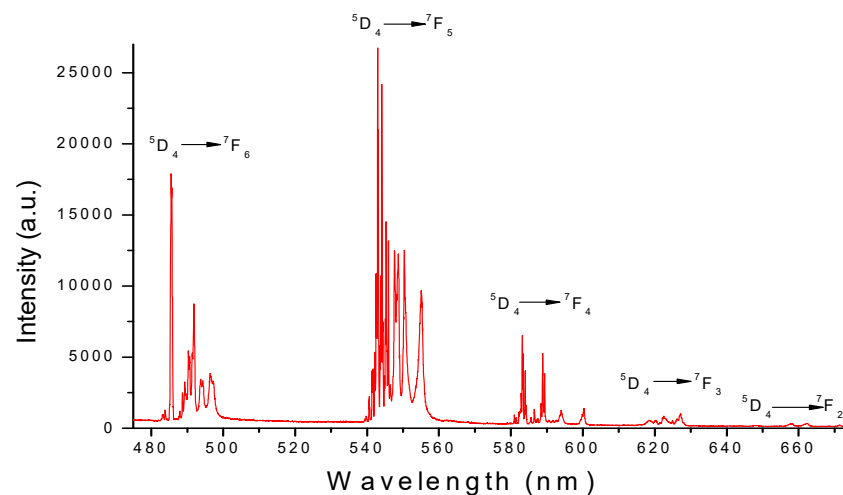
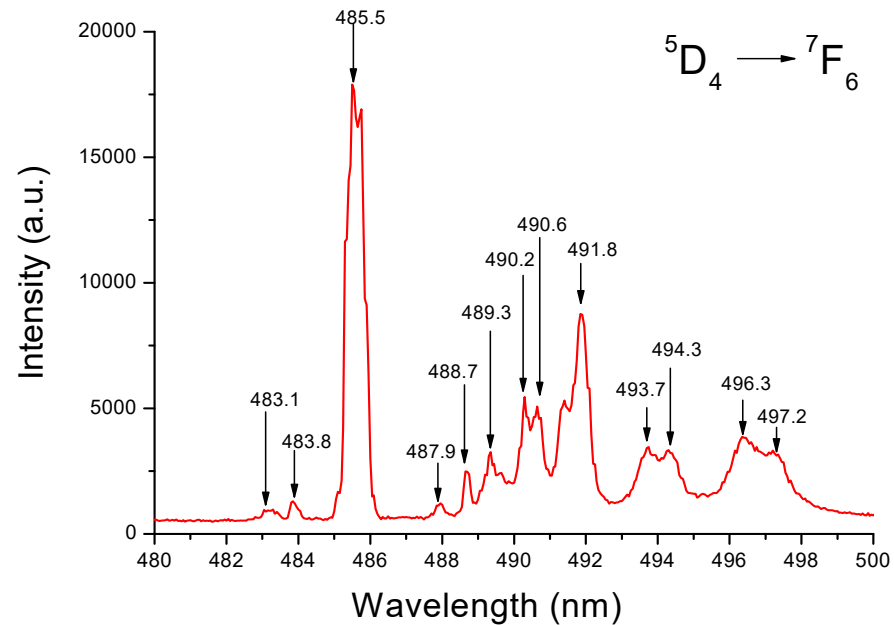
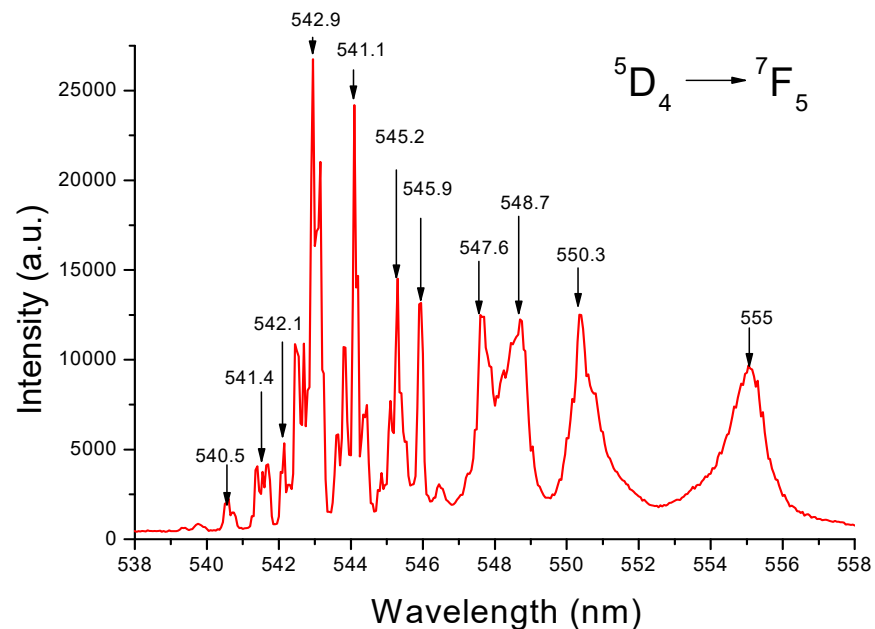


Figure 3. General pattern of the emission spectrum of $YTaO_4:Tb^{3+}$ under 325 nm He-Cd laser excitation at 10 K.

The most intensive part of the spectrum is represented by the series of lines related to the transitions ${}^5D_4 \rightarrow {}^7F_5$ for which $|\Delta J| = 1$ that means that they belong to the allowed transitions in a free ion. The fine structure in each part is caused by the crystal field splitting with possible participation of the vibronic sidebands. Fragments of the energy transitions ${}^5D_4 \rightarrow {}^7F_J$ ($J = 6, 5, 4, 3$) and the pattern optical lines are given in Figure 4a–d. The remaining allowed transitions $J = 2, 1, 0$ which appear under 325 nm excitation proved to be very weak and for this reason were not taken into consideration.



(a)



(b)

Figure 4. Cont.

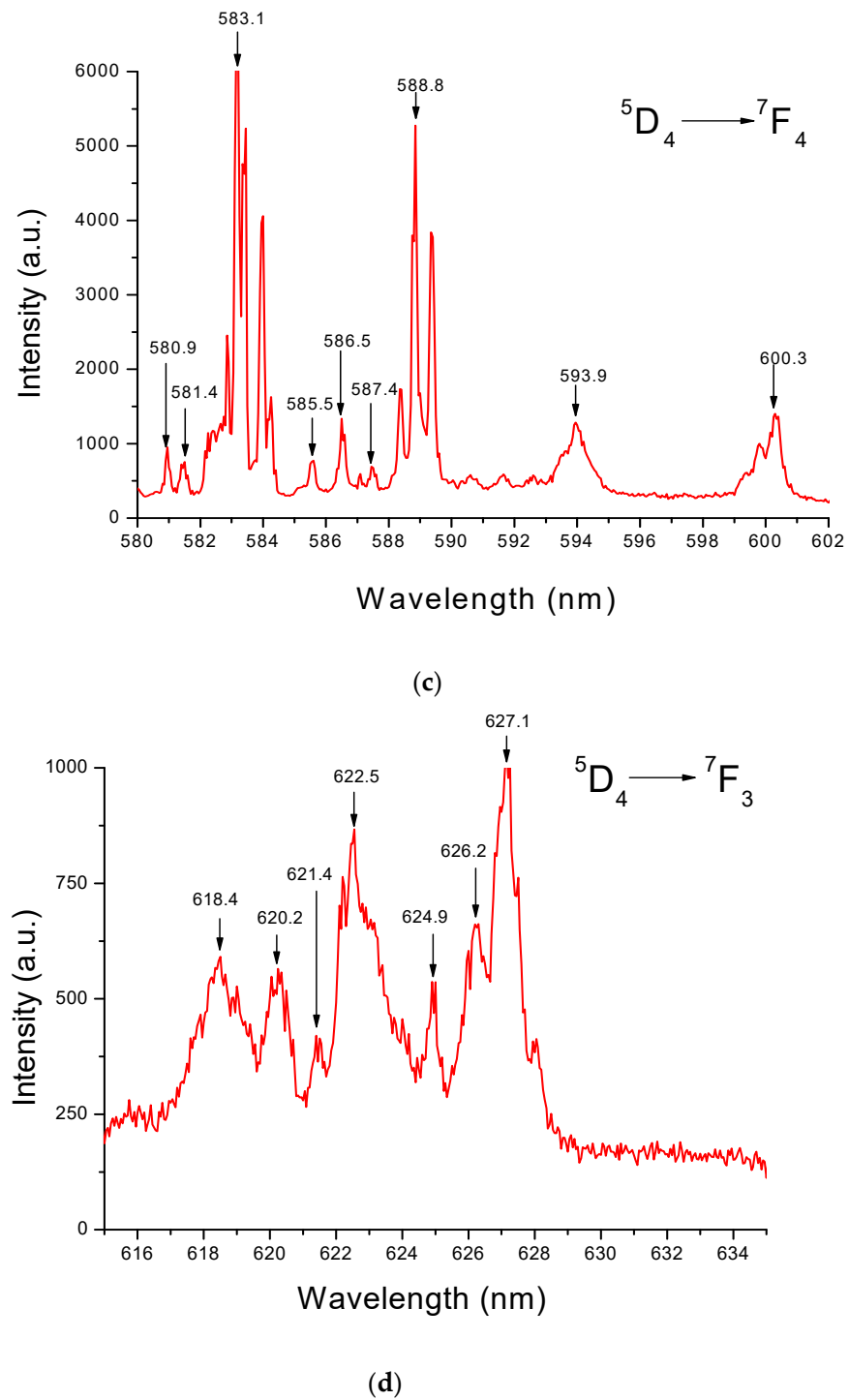


Figure 4. (a) Distribution of the optical lines in ${}^5D_4 \rightarrow {}^7F_6$ transition in $YTaO_4:Tb^{3+}$ at 10 K. (b) Distribution of the optical lines in ${}^5D_4 \rightarrow {}^7F_5$ transition in $YTaO_4:Tb^{3+}$ at 10 K. (c) Distribution of the optical lines in ${}^5D_4 \rightarrow {}^7F_4$ transition in $YTaO_4:Tb^{3+}$ at 10 K. (d) Distribution of the optical lines in ${}^5D_4 \rightarrow {}^7F_3$ transition in $YTaO_4:Tb^{3+}$ at 10 K.

3.2. Experimental Results for $YTaO_4:Eu^{3+}$

The main transitions ${}^5D_0 \rightarrow {}^7F_J$ ($J = 1, 2, 3, 4$) and the pattern of optical lines are given in Figure 5a–d. The remaining transitions $J = 5, 6$, which appear under 325 nm excitation proved to be very weak and for this reason were not taken into consideration.

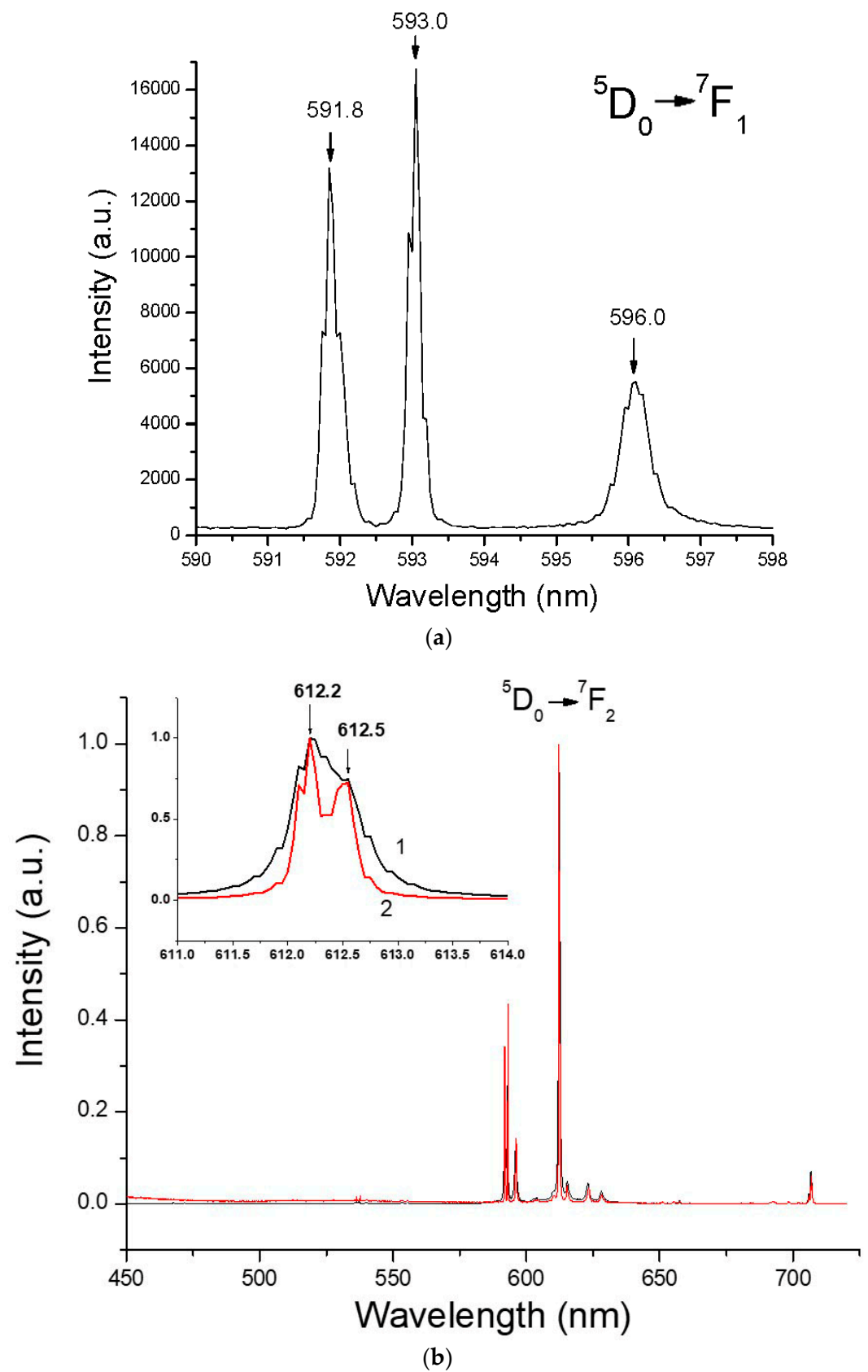
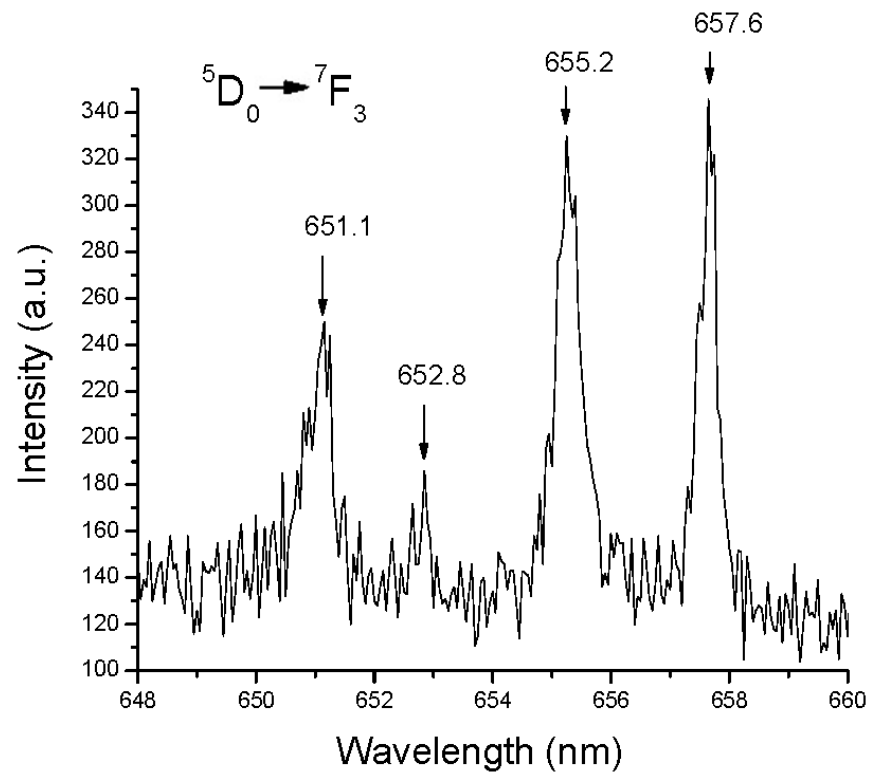
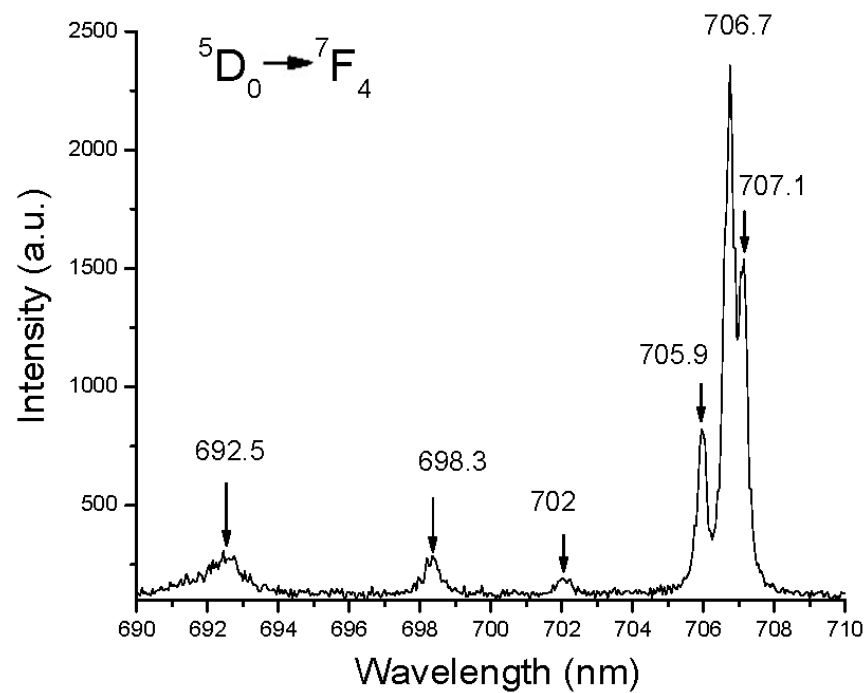


Figure 5. Cont.



(c)



(d)

Figure 5. (a) Distribution of the optical lines in ${}^5D_0 \rightarrow {}^7F_1$ transition in $YTaO_4:Eu^{3+}$ at 10 K. (b) Emission spectra of $YTaO_4:Eu^{3+}$ at room temperature (black line) and 10 K (red line). Insert with the high resolution shows the normalized intensity of the main transition ${}^5D_0 \rightarrow {}^7F_2$ at room temperature (1) and 10 K (2). (c) Distribution of the optical lines in ${}^5D_0 \rightarrow {}^7F_3$ Eu^{3+} transition in $YTaO_4:Eu^{3+}$ at 10 K. (d) Distribution of the optical lines in ${}^5D_0 \rightarrow {}^7F_4$ transition in $YTaO_4:Eu^{3+}$ at 10 K.

In regard to Eu^{3+} activation, only two narrow lines separated at 3 Å can be resolved at 10 K within the main intensive ${}^5D_0 \rightarrow {}^7F_2$ set of transitions under 325 nm He-Cd laser excitation at room temperature (1) and 10 K (2) (Figure 5b).

3.3. Methods of Calculation and Theoretical Results

3.3.1. Nomenclature of Crystal Field Levels of Tb^{3+} and Eu^{3+} Ions in YTaO_4 Crystals

The symmetry of the crystal that is described by discrete point groups is lower than the spherical (full rotation) symmetry of a free ion. According to the well-known quantum-mechanical rules, the energy levels of a free ion undergo splitting in the crystal field. The splitting, i.e., the number of the crystal field sublevels and their symmetry (irreducible representation associated with the eigen-functions) are determined by the symmetry of crystal field and full angular momentum of the ion. The qualitative analysis of the line pattern can be done with the use of the selection rules for the transitions involved. The transitions of the dipole type are allowed under the condition of the low symmetry field which in the present case does not possess an inversion center. Under this condition, the dipole-allowed transitions dominate, meaning that their intensities are much stronger than the magnetic dipole or electric quadrupole ones (see below). In our symmetry-assisted analysis, we will neglect the lines possessing low intensities. The electronic terms of a free rare-earth ion can be well described in Russell–Saunders coupling scheme and therefore the labels as LSJ can be used as the conventional notations. These states of the Tb^{3+} free ion (f^8 -shell) belong to the even irreducible representations (irreps) D_J^+ of the full rotation symmetry group (J is the full angular momentum of the free rare-earth ion, the superscript “+” indicated parity, even” in the case under consideration). The nature of the optical emission and absorption lines of Tb^{3+} in a crystal is usually associated with the following set of transitions between the low-lying levels of Tb^{3+} free ion:

$${}^5D_4 \rightarrow {}^7F_6, {}^7F_5, {}^7F_4, {}^7F_3, {}^7F_2, {}^7F_1, {}^7F_0. \quad (1)$$

The crystal field created by the host lattice results in the splitting of the energy levels of a free ion. Our goal is to qualitatively study the crystal field energy levels and to establish the selection rules and polarization of the lines in crystal field (C_2 point group) of the host lattice for the Tb^{3+} ion. This goal can be reached by the use of the general group-theoretical rule: to reveal the nomenclature of the crystal field levels, one should decompose the irreps D_J^+ in the point group. In compliance with the set of the irreps of C_2 obtained from decomposition of D_J^+ [21], each LSJ multiplet is split into the Stark components labeled accordingly to the irreps of C_2 as A, B (one-dimensional irreps of C_2) [22]. Using the well-known group-theoretical procedure, one can find the following results for the decomposition $D_J^+ \rightarrow$ irreps of C_2 :

$$D_6^+ \rightarrow 7A + 6B, D_5^+ \rightarrow 5A + 6B, D_4^+ \rightarrow 5A + 4B, \quad (2)$$

$$D_3^+ \rightarrow 3A + 4B, D_2^+ \rightarrow 3A + 2B, D_1^+ \rightarrow A + 2B, D_0^+ \rightarrow A. \quad (3)$$

These results allow us find out the nomenclature (irreps) of crystal field multiplets for the Tb^{3+} ion in C_2 point group. Since the C_2 point group has only one-dimensional irreps, A and B the energy levels in crystal field are non-degenerate. Due to the lack of inversion in C_2 , the irreps do not involve the symbol of parity that allows a dipole transition to occur. The results of the group-theoretical classification of the crystal field terms are collected in Table 1.

The general pattern of crystal field splitting of ${}^{2S+1}D_J$ multiplets for Tb^{3+} is shown in Figure 6. One has to mention that the ground term of the Tb^{3+} ion is 7F_6 ($J = 6$).

Table 1. Correspondence between the *LSJ* terms and crystal field levels (irreps) for the Tb^{3+} ion in C_2 point symmetry group.

<i>LSJ</i> terms	5D_4	5D_3	7F_6	7F_5	7F_4
Crystal field terms	$5A + 4B$	$3A + 4B$	$7A + 6B$	$5A + 6B$	$5A + 4B$
<i>LSJ</i> terms	7F_3	7F_2	7F_1	7F_0	
Crystal field terms	$3A + 4B$	$3A + 2B$	$A + 2B$	A	

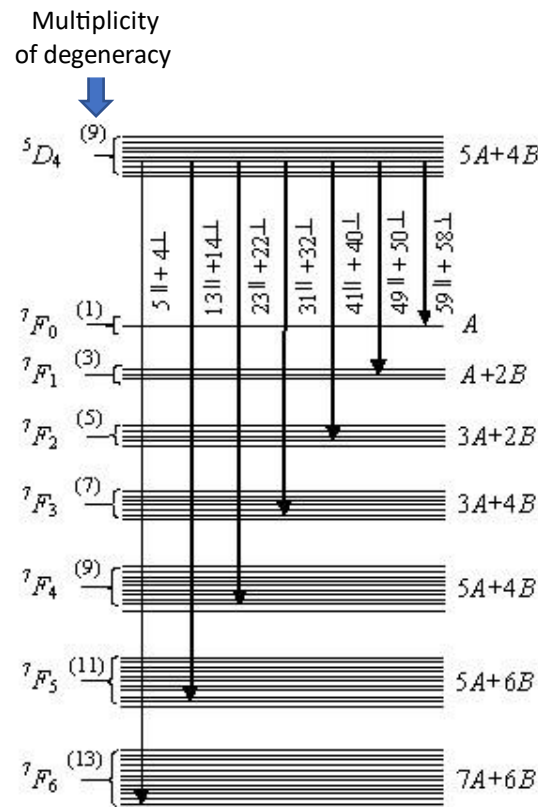


Figure 6. Scheme of the splitting of $^{2S+1}D_J$ multiplets for Tb^{3+} in the crystal field of the C_2 symmetry site with the indication of the optical transitions and their polarization.

3.3.2. Selection Rules for the Allowed Dipole Type Transitions in Tb^{3+} and Eu^{3+} Ions in $YTaO_4$ Crystals

To make more a definite judgment regarding the composition of the optical lines, one can consider the selection rules for the transitions.

Since the set of point symmetry operations does not contain the inversion center, the selection rules do allow the dipole transitions that change the parity of the combined states in the systems containing an inversion center. Under this condition, the allowed dipole type transitions are the most intensive and therefore play a dominant role in the optical spectrum (see, for example, Ref. [23]). The components of the dipole moment are transformed accordingly to the irreps A and B : $d_z \rightarrow A$, $d_x, d_y = B$ that define the disposition of the polarization vector. The selection rules for the allowed transitions and their polarizations can be found from the direct products of irreps of C_2 for the two levels involved in the optical transition [24,25]; $A \times A = A$, $B \times B = B$, $A \times B = B$. Therefore, we can distinguish between the transitions in z-polarization (vector polarization is aligned along C_2 axis) and in x, y-polarization (polarization vector directed in plane perpendicular to C_2). We will call them “parallel” and “perpendicular” polarizations, respectively, according to the components of the dipole moment involved in the transition. In this way, we arrive at the

conclusion that $A \leftrightarrow A$ and $B \leftrightarrow B$ transitions have “parallel” (\parallel) polarization, while $A \leftrightarrow B$ lines have “perpendicular” (\perp) polarization.

The illustrative scheme in Figure 6 qualitatively provides a picture of possible number of the lines allowed in \parallel and \perp polarizations and a qualitative pattern of the crystal field components in the spectrum for Tb^{3+} . It is to be underlined that the energy gaps or alternatively, intervals, separating crystal field levels cannot be determined on the basis of symmetry solely, but the group-theoretical consideration lies at the background of the ab initio evaluation of the crystal field parameters and positions of the lines in the spectral pattern (this task has been solved in our paper [23] devoted to consideration of $SrAl_2O_4:Eu^{2+}$ phosphor). In particular, the dimensions of the matrices of the crystal field operators can be reduced if one used the wave functions spanning the irreps of C_2 group. Actually, the rank of the crystal field matrices to be diagonalized is equal to the number of the repeated (the same) representations that is lower than the dimension of the full Hilbert space.

To solve this problem of the energy pattern, it is also required to get some additional data such as the relative intensities. In particular, some lines are allowed according to the symmetry rules, but their intensities could be small. Some useful conclusions can be deduced under the realistic assumption that only the low-lying crystal field sublevel originated from the 5D_4 term is populated. At very low temperatures, this can be either an A or B level. For instance, if the ground sublevel is A , we have only the line corresponding to the transition $A \leftrightarrow A$ (that has \parallel polarization) in the spectral region corresponding to $^5D_4 \rightarrow ^7F_0$ lines. A similar scheme of the levels for the Eu^{3+} ion ($4f^6$) is illustrated in Figure 7.

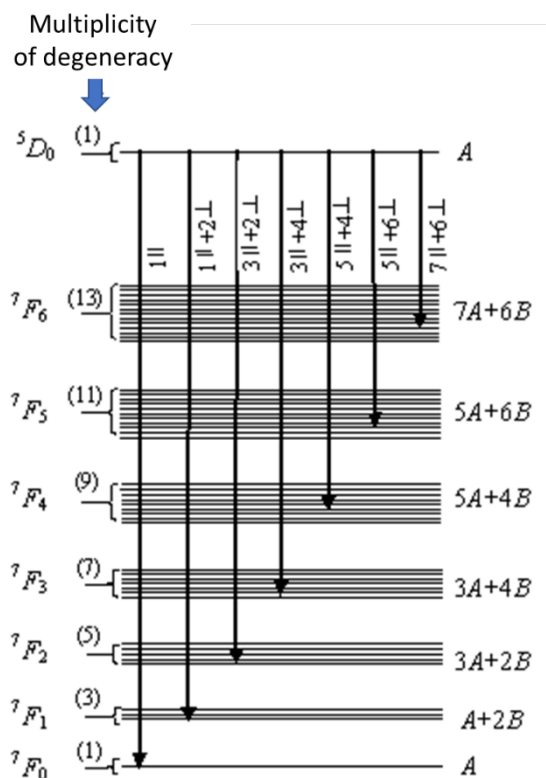


Figure 7. Schematical view of crystal field components of $^{2S+1}D_J$ multiplets for Eu^{3+} in the C_2 symmetry position with the indication of the optical transitions and their polarization.

One can observe that the order of the low-lying levels is reversed with respect to that in Tb^{3+} ($4f^8$). Now, the ground state is 7F_0 ($J = 0$), which gives rise to a singlet A in the crystal field. The correspondence of the crystal field sublevels and LSJ multiplets is similar to that that has been already considered and listed in Table 1. Considering the selection rules revealed so far, one can draw for the Eu^{3+} ion a scheme of transitions shown

in Figure 7. It is to be noted that in high energy areas of the optical pattern, one can observe the only weak line ($A \rightarrow A$) polarized along C_2 axis.

3.3.3. Selection Rules for the Vibronic Satellites: Symmetry-Assisted Approach

Up until now, we have considered the selection rules for the purely electronic (zero-phonon) lines, thus neglecting the electron-vibrational (vibronic) interaction. This approximation is satisfactory for the transitions within the crystal field terms arising from the $4f^n$ configurations of rare-earth ions for which the vibronic coupling is small (that means that heat release Pekar–Huang parameter is in the order of 0.01–0.1) That means that the zero-phonon lines are strong enough at the background of the full electron-vibrational spectra. The situation of a weak vibronic coupling is common for the f-f transitions in rare-earth ions. From the experimental point of view, this is confirmed by the fact that these transitions are represented by the most intensive zero-phonon lines and relatively weak phonon satellites. This statement also has a clear physical background. Indeed, the f-shells are well screened by filled shells and therefore weakly coupled to phonons. Even in this case of a weak vibronic coupling along with the zero-phonon lines, the full spectrum includes vibronic satellites having the intensities that allow one to observe them along with the zero-phonon lines. They are especially important when the zero-phonon lines are forbidden by symmetry and vibrational lines are narrow (this occurs when the local or pseudo-local vibrations are active). That is why the full spectrum characterization requires analysis of the vibronic satellites. The active frequencies can be independently analyzed by means of Raman and IR spectroscopy methods.

At this stage of study, we will discuss the symmetry-related aspects of this problem that is the derivation of the selection rules for the vibronic satellites. Since the vibronic coupling is small, it can be taken into account within the second-order perturbation theory along with the dipole type electron–photon interaction. The complex matrix element (amplitude of transition) within the second-order perturbation theory includes virtual transitions through the excited levels of the electron-vibrational levels (1 and 2) that can be expressed as:

$$\sum_i \frac{\langle \Gamma_2 \gamma_2, n_k | \mathbf{ud} | \Gamma_i \gamma_i, n_k \rangle \langle \Gamma_i \gamma_i, n_k | V_k(\mathbf{r}) Q_k | \Gamma_1 \gamma_1, n_k \pm 1 \rangle}{E_i - E_1} + \sum_j \frac{\langle \Gamma_2 \gamma_2, n_k | V_k(\mathbf{r}) Q_k | \Gamma_j \gamma_j, n_k \pm 1 \rangle \langle \Gamma_j \gamma_j, n_k \pm 1 | \mathbf{ud} | \Gamma_1 \gamma_1, n_k \rangle}{E_j - E_1}. \quad (4)$$

In Equation (4) the term \mathbf{ud} denotes the interaction of the electronic shell (r is the set of the electronic coordinates, \mathbf{d} —dipole moment) with the photon having polarization vector \mathbf{u} , Γ_1 , and Γ_2 are the irreps corresponding two electronic states (irreps A and B in the case under consideration), γ_1 and γ_2 are the symbols numerating basis functions (they are introduced for the purpose of generality but in our case of non-degenerate irreps these symbols are not required). The expression $V_k(\mathbf{r})Q_k$ describes the electron–phonon coupling with vibrational mode k (index combining irrep Γ_k and basis γ_k) having normal coordinate Q_k , n_k is the vibrational quantum number that changes in in the processes of the light absorption (emission), $n_k \rightarrow n_k \pm 1$. This is evidence of the fact that the complex (second-order) perturbation describes the vibronic satellites of the zero-phonon lines. Finally, E_i are the energies of the excited levels virtually participating the second-order perturbation theory.

The complex matrix element (corresponding amplitude A_{12}), Equation (4), corresponding to optical process accompanied by the absorption/emission of the vibrational quantum, can be written as:

$$A_{12}(\Gamma_1 \rightarrow \Gamma_2, n_k \rightarrow n_k \pm 1) = \frac{2}{\Delta E} \langle \Gamma_2 \gamma_2, n_k \pm 1 | \mathbf{ud} \times V_k(\mathbf{r}) Q_k | \Gamma_1 \gamma_1, n_k \rangle. \quad (5)$$

Since the energies of the excited levels in Equation (4) exceed the crystal field gaps considerably, the energy gaps $E_j - E_1$ can be substituted by the mean values ΔE .

Let us analyze the symmetrical properties of the effective operator inducing vibronic satellites. The direct products of irreps $\Gamma(\mathbf{d}) \times \Gamma_k$ form a set of the reducible representation that can be decomposed into the irreps $\bar{\Gamma}_i$ (for each vibration k):

$$\Gamma(\mathbf{d}) \times \Gamma_k = \sum_i \bar{\Gamma}_i. \quad (6)$$

It is to be noted that $\Gamma(\mathbf{d})$ can also contain one, two, or three irreps (as a vector components in the point symmetry group), so that the product in Equation (5) should be considered for each irrep from $\Gamma(\mathbf{d})$. Then, one can formulate the selection rule for the vibronic satellites: the vibronic line corresponding to the transition $\Gamma_1 \leftrightarrow \Gamma_2$ with participation of the vibration Γ_k is allowed if the direct product $\Gamma_1 \times \Gamma_2$ contain at least one irrep $\bar{\Gamma}_i$, or symbolically $\Gamma_1 \times \Gamma_2 \subset \bar{\Gamma}_i$. This condition can be expressed in an alternative form: $\Gamma_1 \times \Gamma_2 \subset \Gamma(\mathbf{d}) \times \Gamma_k$.

Let us illustrate application of the symmetry by considering of the transition $A \leftrightarrow A$ that is allowed in \parallel polarization ($\Gamma(d_z) = A$). For the vibration of B -symmetry, application of the rule as formulated so far shows that the vibrational satellite is allowed in \perp polarization. The remaining transitions can be considered in a similar way. This allows one to treat the vibronic spectrum and gives powerful tool to assign the observed lines to the transitions of a certain type. To realize possibilities provided by the theoretical analysis of the vibronic satellites, polarization measurements are required. The temperature dependence of the lines intensities is also useful because it can provide an additional option to discriminate Stokes and anti-Stokes lines. Independently, the analysis of the vibrational (infrared and Raman) spectra can provide information about the frequencies and symmetry vibrational modes that are observable in optical spectra.

4. Discussion

According to Ofelt's [24] (see also Ref. [25]) theory of the energy levels and wave functions of the free Tb^{3+} ion, the main transitions for Tb^{3+} originate from highest excited level $^5\text{D}_4$ down to the low-lying levels $^7\text{F}_J$ ($J = 6, 5, 4, 3, 2, 1, 0$). The energy levels of a free ion undergo splitting under the action of the crystal field of the host lattice that have been observed. The $^5\text{D}_4 \rightarrow ^7\text{F}_5$ transition located at about 550 nm has a dominating intensity, giving rise to a strong green luminescence. However, the intensities of the $^5\text{D}_4 \rightarrow ^7\text{F}_6$, $^7\text{F}_4$, $^7\text{F}_3$ are rather small but their contributions should also be considered, while the intensities of the transitions $^5\text{D}_4 \rightarrow ^7\text{F}_2$, $^7\text{F}_1$, $^7\text{F}_0$ are negligible.

The crystal field splitting depends on the nature of the host lattice, and for Tb^{3+} and Eu^{3+} in YTaO_4 (C_2 point group) the transitions are schematically shown in Figures 6 and 7. We could not detect the fine structure of this splitting at room temperature because of the temperature effects (such as thermal broadening), but in the case of low-temperature measurements, this splitting was clearly observed as shown in Figure 4.

The Stark components of Tb^{3+} considered in the theoretical treatment have been observed in the low-temperature measurements and indicated in the Figures 5–7: $^7\text{F}_6$ level is split into 13 sublevels; $^7\text{F}_5$ level gives rise to 11 peaks, $^7\text{F}_4$ level leads to 9 resolved peaks, $^7\text{F}_3$ level includes 7 peaks, etc. Moreover, one can also observe the fine structure of the spectrum. Most of these sublevels have a complicated structure arising from the crystal field effects. This is a result of the pseudo-degeneracy of excited level $^5\text{D}_4$, or further splitting of $^7\text{F}_J$ levels.

More detailed analysis of the fine structure of the levels can be done with the use of the explicit expression of the crystal field potentials in terms of allowed (in C_2 symmetry) harmonics and diagonalization of the corresponding matrices. Since the symmetry is low the number of the independent semiempirical parameters is large, so the results of the semiempirical theory are expected to be flexible. In this respect, the semiempirical approach should be supplemented by the ab initio calculation of the crystal field parameters to ensure required accuracy of the comparison of the theoretical results with the experimental ones.

At the same time, the proposed method of the identification of the vibronic lines has not been explored yet. This work is planned.

5. Conclusions

We have analyzed a qualitative picture of the splitting of $^{2S+1}D_J$ multiplets for Tb^{3+} and Eu^{3+} in the crystal field of C_2 symmetry. We have found the selection rules for the transition between crystal field sublevels in Tb^{3+} and Eu^{3+} in the C_2 site symmetry. Using the group-theoretical approach, we have analyzed the polarization rules for the allowed dipole transitions. Low-temperature PL measurements show good correlation with theoretical calculation for Tb^{3+} luminescence and weak splitting for Eu^{3+} luminescence. The observed spectra are in a good correlation with the numbers of the lines revealed through the group-theoretical analysis. We propose that further progress in the symmetry-assisted analysis of the optical spectra can be achieved through the analysis of the vibrational satellites of the zero-phonon lines that is expected to be efficient due to small vibronic interactions for the f-f transitions in rare-earth ions. The selection rules for the vibronically assisted lines were shown to be different from those corresponding to the purely electronic transitions. More sophisticated methods are interrelated with two-photon spectroscopy that provides essentially different selection rules for the transitions and a specific angular (polarization) dependence for the allowed transitions. The theory is developed in fundamental works of Inoue and Toyazawa [26], Bader and Gold [27], and subsequent studies [28]) (see also detailed presentation of the theory in Ref. [21]). This approach essentially based on symmetry extends possibilities of spectroscopy towards detailed analysis of the optical transitions and practical applications of the luminescent materials.

Author Contributions: Conceptualization, M.N. and B.T.; methodology, M.N. and B.T.; writing—original draft preparation, M.N.; formal analysis, validation, M.N. and B.T.; methodology, B.T.; funding acquisition, M.N. All authors have read and agreed to the published version of the manuscript.

Funding: This research was funded by the ANCD National Research Program (M.N., project no. 20.80009.5007.19).

Data Availability Statement: The data (experimental and theoretical) underlying the results presented in this paper are not publicly available at this time, but may be obtained from the authors upon reasonable request.

Conflicts of Interest: The authors declare no conflict of interest.

References

1. Wolten, G.M. The structure of the M' -phase of $YTaO_4$, a third Fergusonite polymorph. *Acta Crystallogr.* **1967**, *23*, 939–944. [[CrossRef](#)]
2. Brixner, L.H.; Chen, H.Y. On the structural and luminescent properties of the M' $LnTaO_4$ rare earth tantalates. *J. Electrochem. Soc.* **1983**, *130*, 2435–2443. [[CrossRef](#)]
3. Kazakova, L.I.; Dubovsky, A.B.; Semenkovich, G.V.; Ivanova, O.A. Luminescence of $YTaO_4$ single crystals. *Radiat. Meas.* **1995**, *24*, 359–360. [[CrossRef](#)]
4. Fu, Y.; Wang, X.; Peng, M. Tunable photoluminescence from $YTaO_4:Bi^{3+}$ for ultraviolet converted pc-WLED with high chromatic stability. *J. Mater. Chem. C* **2020**, *8*, 6079–6085. [[CrossRef](#)]
5. Hwang, M.H.; Kim, Y.J. Luminescent properties of Eu^{3+} -doped $YTaO_4$ powders. *Ceram. Int.* **2008**, *34*, 1117–1120. [[CrossRef](#)]
6. Popovici, E.-J.; Nazarov, M.; Muresan, L.; Noh, D.Y.; Morar, M.; Bica, E.; Indrea, E. Studies on terbium activated yttrium based tantalate phosphors. *Radiat. Meas.* **2010**, *45*, 300–303. [[CrossRef](#)]
7. Cho, S. Synthesis and Luminescence Properties of $YTaO_4:RE^{3+}$ ($RE = Eu, Dy$) Phosphors. *J. Korean Phys. Soc.* **2019**, *74*, 707–712. [[CrossRef](#)]
8. Hu, B.; Hong, G.-Y.; Gan, S.-C.; Kong, L. Preparation and luminescence properties of $YTaO_4:Gd, Eu$. *Chin. J. Lumin.* **2009**, *30*, 601–605.
9. Nan, S.; Hong, F.; Xu, H.; Dou, J.; Liu, G.; Dong, X.; Wang, J.; Yu, W. Luminescence properties and energy transfer of Tb^{3+} , Eu^{3+} co-doped $YTaO_4$ phosphors obtained via sol-gel combustion process. *J. Mater. Sci. Mater. Electron.* **2020**, *31*, 13688–13695. [[CrossRef](#)]
10. Serdar, Y.; Selim, D.; Kadriye, E.; Erdal, C.; Zumre, A. Production, characterization, and luminescent properties of Eu^{3+} doped yttrium niobate–tantalate films. *J. Adv. Ceram.* **2017**, *61*, 33–42.

11. Si, W.; Tehrani, Z.P.; Haydous, F.; Marzari, N.I.; Castelli, E.; Pergolesi, D.; Lippert, T. Yttrium Tantalum Oxynitride Multiphases as Photoanodes for Water Oxidation. *J. Phys. Chem. C* **2019**, *123*, 26211–26217. [[CrossRef](#)]
12. Borges, F.H.; Martins, J.C.; Caixeta, F.J.; Pereira, R.R.; Carlos, L.D.; Ferreira, R.A.S.; Gonçalves, R.R. Primary thermometers based on sol–gel upconverting Er³⁺/Yb³⁺ co-doped yttrium tantalates with high upconversion quantum yield and emission color tunability. *J. Sol-Gel Sci. Technol.* **2022**, *102*, 249–263. [[CrossRef](#)]
13. Blasse, G.; Brill, A. Luminescence phenomena in compounds with fergusonite structure. *J. Lumin.* **1970**, *3*, 109–131. [[CrossRef](#)]
14. Lammers, M.J.J.; Blasse, G. Energy transfer phenomena in Tb³⁺-activated gadolinium tantalite. *Mater. Res. Bull.* **1984**, *19*, 759–768. [[CrossRef](#)]
15. Blasse, G. Vibrational spectra of yttrium niobate and tantalate. *J. Solid State Chem.* **1973**, *7*, 169–171. [[CrossRef](#)]
16. Nazarov, M. Color cathodoluminescence of yttrium tantalate activated by europium and terbium. *J. Surf. Investig. X-ray Synchrotron Neutron Tech.* **2022**, *16*, 770–774. [[CrossRef](#)]
17. Shannon, R.D. Revised Effective Ionic Radii and Systematic Studies of Interatomic Distances in Halides and Chalcogenides. *Acta Crystallogr. Sect. A Cryst. Phys. Diffr. Theor. Gen. Crystallogr.* **1976**, *A32*, 751–767. [[CrossRef](#)]
18. Hristea, A.; Popovici, E.J.; Muresan, L.; Stefan, M.; Grecu, R.; Johansson, A.; Boman, M.J. Morpho-structural and luminescent investigations of niobium activated yttrium tantalate. *Alloys Compd.* **2009**, *471*, 524–529. [[CrossRef](#)]
19. Nazarov, M.V.; Noh, D.Y. *New Generation of Europium and Terbium Activated Phosphors from Synthesis to Application*; Pan Stanford Publishing: Singapore, 2011.
20. Issler, S.L.; Torardi, C.C. Solid state chemistry and luminescence of X-ray phosphors. *J. Alloys Compd.* **1995**, *229*, 54–65. [[CrossRef](#)]
21. Tsukerblat, B.S. *Group Theory in Chemistry and Spectroscopy*; Dover Pub.: Mineola, NY, USA, 2006.
22. Koster, G.F.; Dimmok, J.O.; Wheeler, R.G.; Statz, H. *Properties of the Thirty-Two Point Groups*; MIT Press: Cambridge, MA, USA, 1963.
23. Nazarov, M.; Brik, M.G.; Spassky, D.; Tsukerblat, B. Crystal field splitting of 5d states and luminescence mechanism in SrAl₂O₄:Eu²⁺ Phosphor. *J. Lumin.* **2017**, *182*, 79–86. [[CrossRef](#)]
24. Ofelt, G.S. Structure of the f⁶ configuration with application to rare-earth ions. *J. Chem. Phys.* **1963**, *38*, 2171–2179. [[CrossRef](#)]
25. Galler, A.; Pourovskii, L.V. Electronic structure of rare-earth mononitrides: Quasiatomic excitations and semiconducting bands. *New J. Phys.* **2022**, *24*, 043039. [[CrossRef](#)]
26. Inoue, M.; Toyazawa, Y. Two-photon absorption and energy band structure. *J. Phys. Soc. Japan* **1965**, *20*, 363–374. [[CrossRef](#)]
27. Bader, T.R.; Gold, A. Polarization dependence of two-photon absorption in solids. *Phys. Rev.* **1968**, *171*, 997–1003. [[CrossRef](#)]
28. Rajasree, K.S.; Gupta, R.K.; Gokhroo, V.; Kien, F.L.; Nieddu, T.; Ray, T.; Chormaic, S.N.; Tkachenko, G. Spin selection in single-frequency two-photon excitation of alkali-metal atoms. *Phys. Rev. Res.* **2020**, *2*, 033341. [[CrossRef](#)]

Disclaimer/Publisher’s Note: The statements, opinions and data contained in all publications are solely those of the individual author(s) and contributor(s) and not of MDPI and/or the editor(s). MDPI and/or the editor(s) disclaim responsibility for any injury to people or property resulting from any ideas, methods, instructions or products referred to in the content.